JMLR: Workshop and Conference Proceedings 101:972–986, 2019 ACML 2019

Nuclei segmentation by using convolutional network with distance map and contour information

Xiaoming Liu LXMSPACE@GMAIL.COM
Zhengsheng Guo GUOZS7827@163.COM
Bo Li LIBEROL@126.COM
Jun Cao JONAHCAO0109@GMAIL.COM
College of Computer Science and Technology, Wuhan University of Science and technology, Wuhan, 430065, China.
Hubei Province Key Laboratory of Intelligent Information Processing and Real-time Industrial System, Wuhan, 430065, China

Editors: Wee Sun Lee and Taiji Suzuki

Abstract

Accurate access to nuclear information on digital pathology images can assist physicians in diagnosis and subsequent treatment. The pathological images have a large number of nuclei and part of nuclei is touching, manual segmentation is time consuming and error prone. Therefore it is an important task to develop a accurate nuclei segmentation method. For traditional methods, it is hard to obtain a accurately nuclei segmentation result, because the nuclei have many different characterizations. In this paper, we propose a new nuclei segmentation method (MDC-Net), which is a deep fully convolutional network. The network contains multiple residual operations to reduce detail loss in image. In addition, dilated convolution which has different dilation ratio is used to increase receptive field. MDC-Net contains the distance map and contour image, enhancing information on individual nuclei to get accurate segmentation results. We improve the segmentation effect by using the post-processing operate. We demonstrate that MDC-Net can obtain state-of-the-art results on public dataset with multiple organ slices compared with other popular methods.

Keywords: digital pathology, histopathology image analysis, deep learning, nuclei segmentation

1. Introduction

It is important to grade cancer in medicine, doctor can use this information to effectively treat the patient and evaluate the treatment effect (Filipczuk et al. (2013)). Histopathology images are mainly used in clinical medicine and are widely used in the diagnosis and prediction of tumors because they usually include information about the structure of the tumor and tissues. For tissue slices, hematoxylin-eosin (H&E) is usually used for staining, which can separate the nucleus and cytoplasm and highlight structural information such as nuclei. The clinicians can grade the cancer by analyzing the nuclear morphological features in the slices (Naik et al. (2008)).

Computer Aided Diagnosis (CAD) has achieved rapid development in digital pathology. Traditional cancer diagnosis requires manual labeling of tissue slices, this is a time-

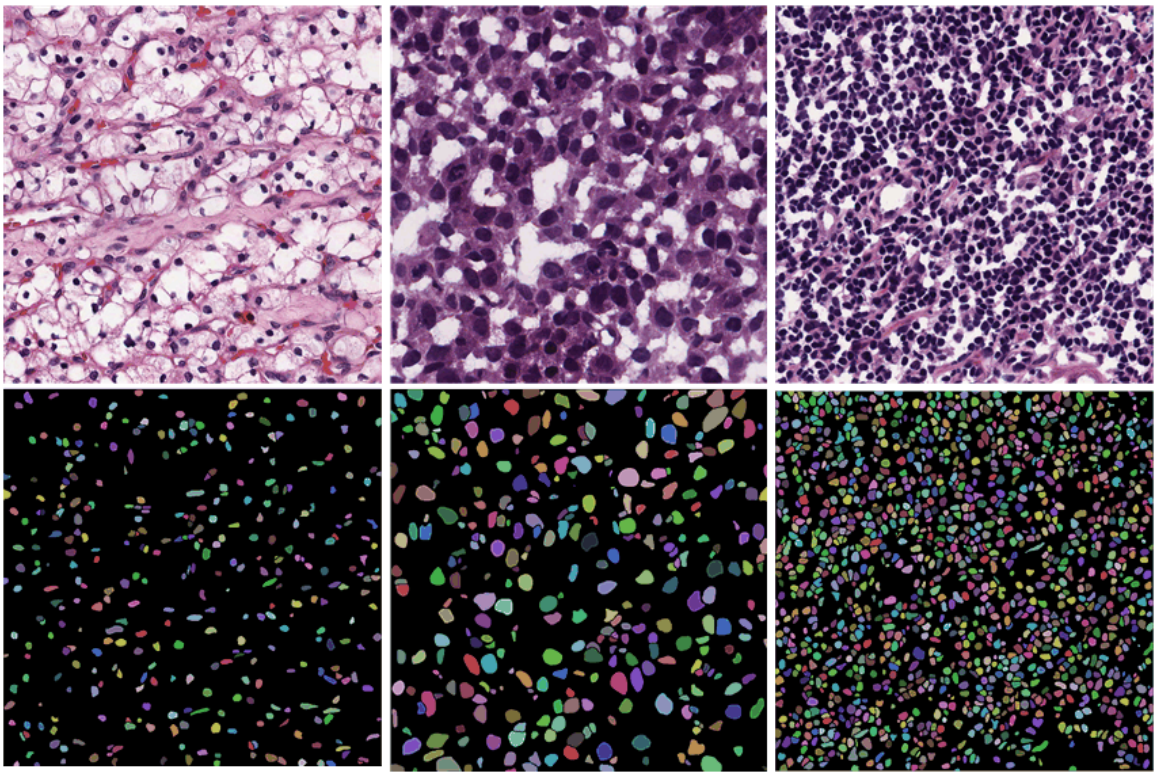

Figure 1: Examples of pathological images, the first row is the pathological image which is staining by H&E, the second row is the corresponding ground truth. The three columns from left to right are the pathological images of the kidney, bladder and stomach respectively.

consuming and error-prone task. Furthermore, manual labeling is a work which influences by subjective of the marker, markers require professional training. In order to ensure the accuracy of the label, more than one marker is needed. So it is importance to find a method which can automatically and accurately segment the nucleus. Some pathology images and ground truth are shown in Figure 1.

There are some challenging problems in nuclei segmentation, but early segmentation method did not consider these problems. For example, in some pathological conditions (hyperplasia etc.), the boundary of nuclei is blurred. Traditional segmentation methods applied to nuclear segmentation are not robust. For example, as Otsu thresholding (Feng et al. (2017)) and marker contorlled watershed (Yang et al. (2006)).

In recent years, convolutional neural network (CNN) is used to medical image processing, including detection and enumeration (Xu et al. (2015)), segmentation (Liu et al. (2018); Abdolhoseini et al. (2019); Al-Kofahi et al.; Liu et al. (2019)), and tissue classification (Sirinukunwattana et al. (2016)). A main challenge in nuclei segmentation is segmenting a large number of overlapping or touching nuclei. Most existing methods cannot solve this problem effectively.

The main contributions of this paper are:

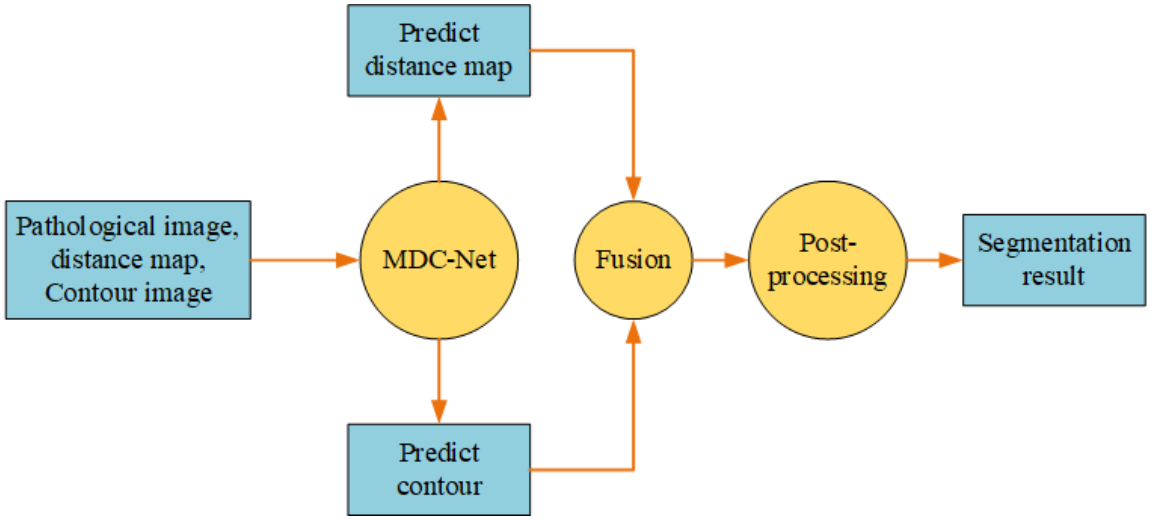

Figure 2: The entire flow chart of our segmentation method.

(1) We propose a new fully convolutional network (MDC-Net) to segment the dense nuclei. MDC-Net contains multi-scale dilated convolution and multi-scale residual operations. The dilated convolution is used to increase receptive field and the residual operation is used to utilize multi-scale of feature maps information.

(2) Our method uses the distance map and contour information to solve the problem which is segmenting touching and overlapping nuclei. We fuse the distance map and contour information to strengthen the morphology and boundary information. And it can effectively alleviated this problem and improve the accuracy of segmentation.

(3) MDC-Net can obtain the state-of-the-art performance on the public nuclei histopathology dataset with multiple organ slices.

2. Related Work

Early medical image segmentation usually used some traditional methods. For example, threshold, clustering (Clark et al. (1994)), edge detection (Davis (1975)). Nuclei information is important in clinical. In recent years, researchers propose many methods, pixel classification (Gao et al. (2016)), mathematical morphology (Cheng et al. (2008)), level sets (Guo et al. (2016)) and graph-based segmentation methods (Xing and Yang (2016)). However, traditional methods are not robust to medical image segmentation.

Recently, some CNN-based methods have been applied to medical image segmentation. Janowczyk et al. (Janowczyk and Madabhushi (2016)) propose a tutorial which show some pathological image target (carcinoma, nuclei, epithelium, tubule) segmentation methods. However,this method used the image patches as the input data. Although using this patch-based approach can achieve better nuclei segmentation results, it is a very time consuming task. Different from this patch-based method, some segmentation methods use the entire pathology image. Naylor et al. (Naylor et al. (2018)) transformed the nuclei segmentation task into a regression task, which can effectively improve the segmentation accuracy of the

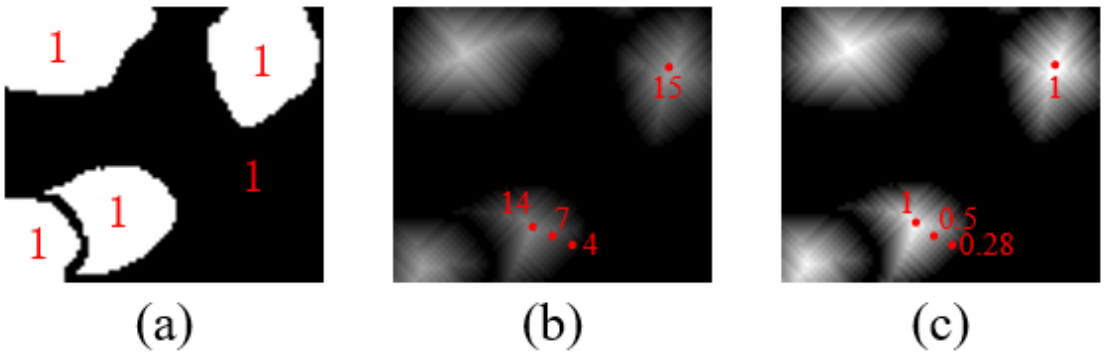

Figure 3: The image which obtain by using chessboard distance transformation to ground truth. (a) ground truth, (b) the distance map which is obtaining by using chessboard distance transformation, (c) normalized distance map, the value of center pixel in each nuclei is 1.

nuclei. There are some segmentation tasks similar to nuclei segmentation in medical image, Chen et al. (Chen et al. (2016)) proposed using contour information to segment the glands. (Raza et al. (2019)) proposed a Micro-Net which is robust in high level noise. Jia et al. (Jia et al. (2017)) proposed a method which uses weak supervision to segment glands.

3. Proposed method

In this section, we introduce and discuss our approach in detail. Firstly, we introduce the pre-processing of datasets. Then, the components of the proposed MDC-Net network and the object loss function are presented. Finally, the post-processing is introduced. The flowchart of the proposed method is shown in Figure 2.

3.1. Data pre-processing

Distance transformation: using the distance transformation to the ground truth can strengthen morphological information of the nuclei and it can improve the effect of nuclei segmentation. In this paper, we apply the chessboard distance transform to the ground truth to obtain the distance map. Finally, we normalize the distance map. And the result of distance map is shown in Figure 3.

Contour information: although using the distance map can strengthen the morphological characteristics of the nuclei, some dense nuclei boundary are still difficult to segment. Thus, we add the contour information to our method to get better nuclei segmentation result.

3.2. Network structure and loss

3.2.1. Overview of network structure

In this paper, we propose a new fully convolutional network named MDC-Net. Firstly using one encoder to extract high-level feature maps from pathological images. And then use two

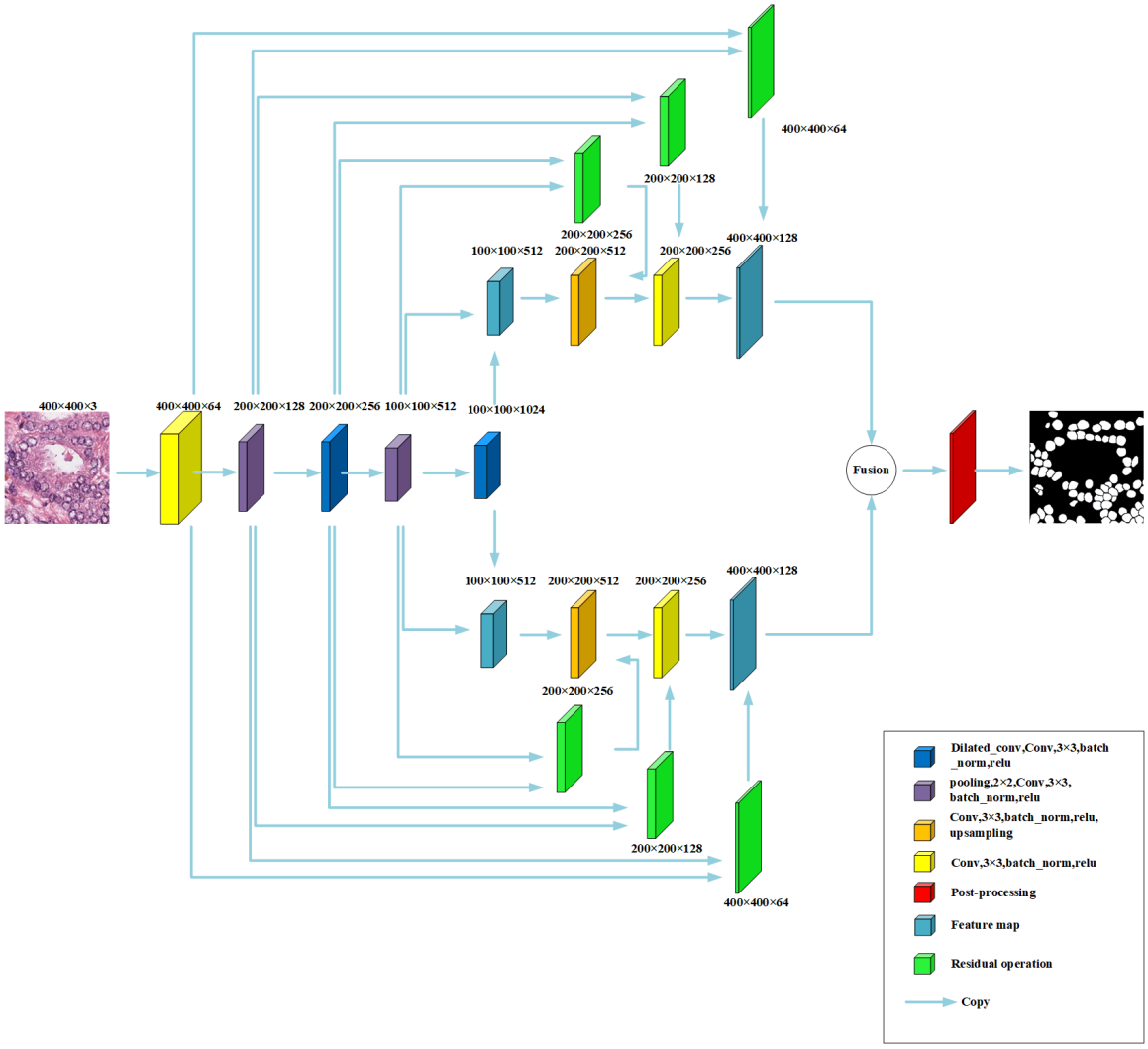

Figure 4: The framework of MDC-Net. The detail of the operate is shown in bottom right corner. The operate of copy is to direct use data.

decoder branches. The first branch is the DM-path, the target is to obtain the predicted distance map. The last branch is the C-path, which uses to get the predicted contour image. The parameters which are in this two branches are independent updated. Using the fusion module to fuse the predicted distance map and contour image. Finally, post-processing is used after the fusion module. The detail of the MDC-Net is shown in Figure 4.

3.2.2. Dilated convolution

Unet (Ronneberger et al. (2015)) is a universal medical image segmentation model. The encoder structure of MDC-Net is similar to U-Net. The pooling layer is used to expand the receptive field of the network, but it will reduce resolution of the feature map. Different from

U-Net, MDC-Net uses dilated convolution(Yu and Koltun (2015)) to enlarge the receptive field in network. In addition, the dilated convolution does not reduce the resolution of the feature map.

Similar to (Chen et al. (2017)), MDC-Net uses the dilation ratio of (1, 2, 5) and uses the dilated convolution in parallel. Different dilation ratios make all of the pixels of image have convolution operation, and can improve the segmentation accuracy.

3.2.3. Residual operations

The residual operation is used to make the network more deeper. These residual operations obtain the output of the entire operation by summing the input and final convolution result. This operation can enhances transmition of information between the layers. By using this residual operation, the detail of the image will be preserved, while it can prevent the gradient vanishing and gradients exploding.

3.2.4. Loss function

The parameter is denoted as W, the result of the DM-path is $P_d = D(W_d)$, and the result of the C-path is $P_c = C(W_c)$. The variable of W_d and W_c are the parameters in DM-path and C-path, respectively. The loss function of the contour is defined as:

$$loss_C = -\sum_{j,k} G_c(j,k) \log(P_c(j,k)) \tag{1}$$

where k is the class in this segmentation task (background and nuclei contour). $j = (x, y)$ is a pixel of an image. $G_c(j,k)$ is the value in ground truth label whether it belongs to k, P_c represents the result of the C-path, and is calculated by softmax. $P_c(j,k)$ represents probability of the pixel belonging to k.

The result from the DM-path is a predicted distance map, the center of the nuclei is defined as a local maximum value in image. The pixel value in distance map represents the normalized distance of the nuclei pixel to the nearest background pixel. The loss function of the DM-path is defined as follows:

$$loss_D = \frac{1}{n} \sum_{j} \left(G_d(j) - P_d(j)\right)^2 \tag{2}$$

where G_d is obtained by using distance transformation in the ground truth (see section 3.1), and P_d is the predicted distance map from the network. j=(x,y) represents a pixel and n is the number of pixels.

There are two parts in the whole loss function, one is the distance map loss and the other is the contour loss. Since the information proportion of nucleus and contour are different on the pathological image, for the two losses we use different weights. These weights are used to balance the nuclei contour and whole nuclei pixels have different proportions in image. The values of these two weights need to be set according to the dataset.

3.3. Fusion module

Fusion module: in order to obtain the final segmentation result, using fusion module to fuse the decoder result of the DM-path (P_d) and C-path (P_c). The fusion formula is defined as follow:

$$fusion(j) = \begin{cases} 1 \text{ if } P_d(j) > t_0 \text{ and } P_c(j) < t_1 \\ 0 \text{ othercases} \end{cases} \tag{3}$$

where t_0 and t_1 are the threshold, and judge pixel is background or nuclei. $j = (x, y)$ is a pixel of image. This operation determines the pixels on the image is the nuclei or background.

3.4. Post-processing

The pixel value in distance map represents the normalized distance of the nuclei pixel to the nearest background pixel. We use the distance transformation to the segmentation map which is same as the pre-processing. Different nuclei have different signal, and this signal has different decline. The detail of this phenomenon of the decline is explained in Soille (2013): R is the probability map. M represent the local maximum in R. M is defined to a nuclei if all path P which is connected M with some higher max maximum $M^{'}$, the decrease value in R is more than the p_1:

$$\min_{\substack{P=(M,..,M') \\ R(M')>R(M)}} \{\max_{x \in P} [R(M) - R(x)]\} > p_1 \tag{4}$$

p_1 is a hyperparameter which can be freely selected, then find nuclei regions by using the watershed transformation seeded from the maxima method in the regions that fulfill this criterion. Furthermore, all object pixels value are required to higher than p_2.

4. Experiment

4.1. Datasets

DATA ORGANS (Naylor et al. (2018)): the pathological tissue slices were obtained with microscope magnified 40× , and using H&E to stained. The resolution of slices are 1000 × 1000 and a total of 30 samples images are extracted from 7 different organs.

4.2. Dividing for datasets

We divide the this dataset into three parts:

Training and Validation dataset: this training and validation data contains four different human organs: prostate, liver, breast and kidney, a total of 16 pathological images. Due to this data does not have many images, we used data augmentation method to expand data. Training dataset has 16 images, and 8 images are used as the validation dataset.

Test dataset A: a total of 8 pathological images in the first test dataset, and contains four human organs: prostate, liver, breast and kidney, and this images not appear in the training dataset.

Test dataset B: different from the test dataset A, this test dataset has 6 pathological images, and has three human organs which are not appear in the training dataset: stomach,

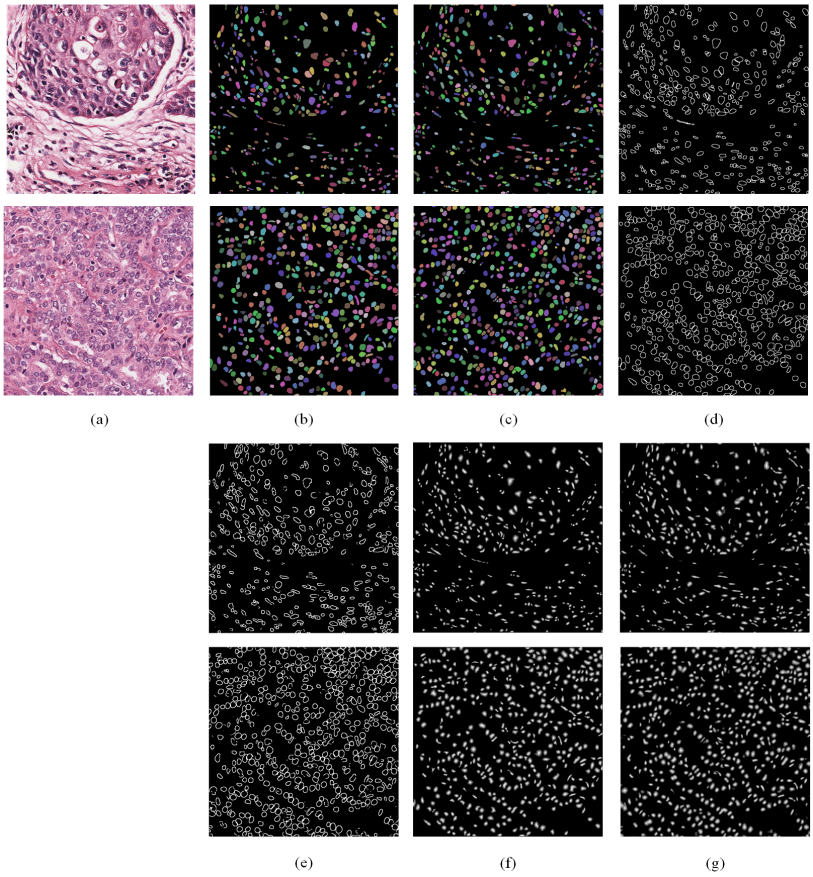

Figure 5: some nuclei segmentation results which use MDC-Net, (a) pathological image, (b) ground truth, (c) the segmentation results, (d) the ground truth of contour, (e) the predicted nuclei contour map, (f) the ground truth of distance map, (g) the predicted distance map.

bladder and colorectal. The purpose of using this dataset is to test the segmentation effect and the generalization of our method for the nuclei in different organs.

4.3. Metrics

For evaluating the segmentation performance of nuclei, we use three indicators. The F1 score is an object-level metric, and the Aggregated Jaccard Index (AJI) (Kumar et al. (2017)) is used for evaluating the segmentation effect in dense nuclei. The Hausdorff distance is used to measure the similarity of the ground truth and predicted image.

The F1 score is a commonly used evaluation index in image segmentation. F1 score is defined as follows:

$$F1 = \frac{2TP}{2TP + FP + FN} \tag{5}$$

TP, FP, FN denote the number of true positives, false positives and false negatives, respectively.

Table 1: comparing the results of nuclei segmentation on the test set in different 7 human organs

		AJI					Hausdorff distance					F1 score				
Human organs	Image	MDC-Net	DIST	U-Net	RefineNet	Mask R-CNN	MDC-Net	DIST	U-Net	RefineNet	Mask R-CNN	MDC-Net	DIST	U-Net	RefineNet	Mask R-CNN
Breast	1	0.5420	0.5350	0.4294	0.3875	0.4353	6.7483	7.0848	7.7268	6.7601	6.6711	0.7747	0.7688	0.7442	0.7446	0.7229
	2	0.5860	0.5257	0.5954	0.5546	0.5262	7.3163	7.8500	7.4889	7.8400	8.3706	0.8274	0.8137	0.8351	0.8067	0.7535
Kidney	1	0.5900	0.5716	0.5868	0.5375	0.5749	5.6811	6.4757	5.6160	5.6210	5.8238	0.7914	0.7790	0.8090	0.7919	0.7723
	2	0.5290	0.5740	0.4695	0.4270	0.4242	6.6350	5.8613	7.4411	6.9184	6.6380	0.7645	0.7676	0.7421	0.7430	0.7020
Liver	1	0.5306	0.5370	0.4660	0.4416	0.4941	6.8185	7.1043	7.5480	6.9615	6.9430	0.7874	0.7740	0.7672	0.7720	0.7489
	2	0.4747	0.4581	0.4603	0.3407	0.4219	11.1732	11.4000	11.1677	11.0853	10.7682	0.7016	0.6838	0.7135	0.5688	0.6246
Prostate	1	0.6085	0.6080	0.3974	0.2233	0.5282	8.2812	8.4356	8.6951	8.2392	7.7229	0.7912	0.7847	0.7842	0.8011	0.7904
	2	0.6529	0.5970	0.5770	0.4352	0.5894	9.5775	9.8192	9.8057	9.6445	9.6970	0.8050	0.7963	0.7962	0.7987	0.7803
Bladder	1	0.6339	0.5741	0.6089	0.5629	0.5947	7.6381	8.0584	7.7908	7.8544	8.1290	0.8502	0.8450	0.8505	0.8554	0.8283
	2	0.4921	0.5542	0.3937	0.4116	0.3901	7.2600	7.1966	8.4421	7.9702	8.1201	0.7736	0.7874	0.7369	0.7419	0.7101
Colorectal	1	0.4457	0.4325	0.3453	0.0861	0.3800	11.7022	11.0443	11.4182	14.1867	11.5746	0.7248	0.7212	0.7444	0.6774	0.6046
	2	0.5000	0.4568	0.4537	0.2125	0.4118	11.2912	11.5262	10.6567	12.3042	11.5386	0.7392	0.7344	0.7689	0.7433	0.6370
Stomach	1	0.5846	0.6455	0.4670	0.4534	0.4920	10.3267	10.0853	10.4201	10.0040	11.0242	0.8306	0.8366	0.8305	0.8466	0.7963
	2	0.6024	0.6385	0.4857	0.4876	0.5525	9.5088	9.5878	9.5773	9.4179	10.1787	0.8410	0.8450	0.8405	0.8476	0.8048
average		0.5551	0.5505	0.4812	0.3972	0.4868	8.5684	8.6806	8.8421	8.9148	8.7999	0.7859	0.7812	0.7830	0.7670	0.7340

The Aggregated Jaccard Index (AJI) is an extension of the global Jaccard Index. The target is to penalize both object-level and pixel-level errors. Firstly, we use maximizing the Jaccard Index to obtain the component of each ground truth, and get the result which is intersection of the component in the ground truth and final segmentation result, adding this result value to the numerator. The denominator is this matched components and union of the undetected component. Finally, the value of AJI is numerator divided by the denominator. The detail of formula is shown as follow:

$$AJI = \frac{\sum_{k=1}^{L} |G_i(k) \cap S_i'(j)|}{\sum_{k=1}^{L} |G_i(k) \cup S_i'(j)| + \sum_{l \in T} |S_i(l)|} \tag{6}$$

$G_i = \bigcup_{k=1...L} G_i(k)$ represents ground truth pixels, $S_i'(j)$ represents the component obtained by in the segmentation result to use maximizing the Jaccard Index. Set T represents a component which is mismatched in ground truth and segmentation result.

Hausdorff distance (Huttenlocher et al. (1992)) is used to measure the distance of pixels between the ground truth and predicted result, and the target is evaluating the similarity between the predicted result image and corresponding ground truth. P represents the final result image, $d(\cdot)$ is the distance of two pixels.

$$H(G,P) = \max[\max_{x_g \in G} \min_{x_p \in P} d(x_g - x_p), \max_{x_p \in P} \min_{x_g \in G} d(x_g - x_p)] \tag{7}$$

4.4. Comparsion with other segmentation methods

We compared the proposed method with other four state-of-the-art methods: Mask R-CNN, U-Net, DIST (Naylor et al. (2018)) and RefineNet (Lin et al. (2017)). We used TensorFlow

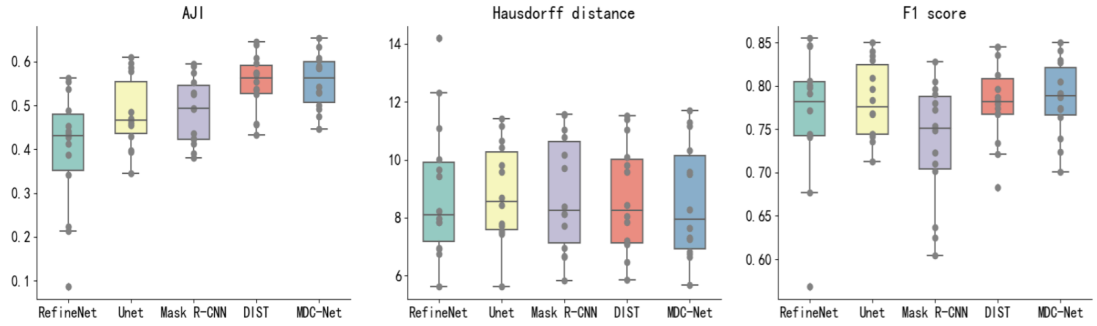

Figure 6: The box plots which are showing the results of nuclei segmentation, and it is obtained by using each segmentation method on the test dataset.

(Abadi et al. (2016)) to build each network structure. The used GPU is GTX1070, and the computer's memory capacity is 8GB. The backbone network in Mask R-CNN and RefineNet use ResNet-101, used pre-trained model in ImageNet to get the initial parameters. The values in DIST was same as (Naylor et al. (2018)), in all segmentation methods, batch_size and learning rate were setting to 2 and 0.0001. The input image size was 512×512 for all methods and maximum epoch was setting to 500. Figure 5 shows typical nuclei segmentation results of the proposed MDC-Net in histopathological images, it shows ground truth, contour, distance map and corresponding predicted images, respectively. These two images are from two organs (Breast, stomach).

Table 1 lists some segmentation results which are using different methods on test dataset A and B. From Table 1 can see that RefineNet and U-Net can obtain better performance on F1 score, but the segmentation result show inferior in Hausdorff distance and AJI. This appearance shows that the different characteristics of segmentation methods can be presented in criterions of the object-level and pixel-level. At the same time, both MDC-Net and DIST method have improved from the fully convolutional network, they can get better results both on F1 and AJI. Box plots of different segmentation results are shown in Figure 6. The outlier points are defined as the point which is result value outside range. Figure 7 shows result of different segmentation method.

The results in Table 1 shows that MDC-Net method can obtain best performance in F1 and Hausdorff distance, the result of AJI is similar to DIST, and the result values are higher than other methods.

We can obtain the conclusion from Table 1 that there is no one segmentation method which can achieve the best performance in every pathological image. Some factors contribute to the problem, such as the nuclei density is not same in pathological images, the difference of nuclei characteristics in some organs are widely. However, the result shows that MDC-Net which uses fully convolutional network, distance map and nuclei contour information can obtain the best result for test datasets.

Table 2: Comparing effect of post-processing

	AJI	Hausdorff distance	F1-score
Not Post-processing	0.5387	8.5820	0.7845
Post-processing before fusion	0.5500	8.5740	0.7820
Post-processing after fusion	0.5551	8.5684	0.7859

Table 3: Comparing methods with no post-processing

	MDC-Net	Mask R-CNN	U-Net	RefineNet
AJI	0.5387	0.4868	0.4811	0.3972
Hausdorff distance	8.5820	8.7999	8.8421	8.8791

4.5. Ablation experiment

4.5.1. Post-processing

In order to investigate the effect of post-processing operations in the segmentation method. The ablation experiment was performed on MDC-Net, and the other operations are the same as previous experiments. The hyperparameters t_0 and t_1 in fusion operation are setting to 0.1 and 0.8, respectively. In this section, we evaluated three different methods. The first method does not include post-processing operations, and gets the result after fusing the contour information and initial segmentation result. The second method uses post-processing operations before the fusion operation, and it only uses in predicted distance map. The last method uses the post-processing after the fusion operation (MDC-Net). The hyperparameters p_1 and p_2 are setting to 1 and 0.1, respectively.

The results are shown in the Table 2, we only show the average of the result in entire test dataset. It can obtain the conclusion from the Table 2 that the post-processing operation can improve AJI value to some extent. Post-processing operations can improve the segmentation effect for overlapping and touching nucleus. Comparing to the method which is not use the post-processing operation, MDC-Net is improved about 2% in AJI. Furthermore, comparing to the method which is using post-processing operations before the fusion operation, MDC-Net is improved about 0.5% in AJI.

The post-processing operation can improve the Hausdorff distance value. This shows for the object-level criterion, the post-processing operation can improve the segmentation result. However, post-processing operation can not get significant improvement for F1 scores. The reasons may be that the post-processing operation mainly improve the contour pixels, while contour pixels make up a small part of the whole nuclei. The post-processing operation has a significant positive effect for the object-level but less in pixel-level.

In order to evaluate the performance of MDC-Net, we removed the post-processing from the MDC-Net. And then comparing with U-Net, Mask R-CNN and RefineNet on AJI and Hausdorff distance. We set the hyperparameters of t_0 and t_1 are 0.1 and 0.8 for fusion module. The detail of segmentation result is shown in Table 3. The result of Table 3 can conclude that our proposed MDC-Net without the post-processing can get better effect in AJI and Hausdorff distance compare to other state-of-the-art method. It can be proved

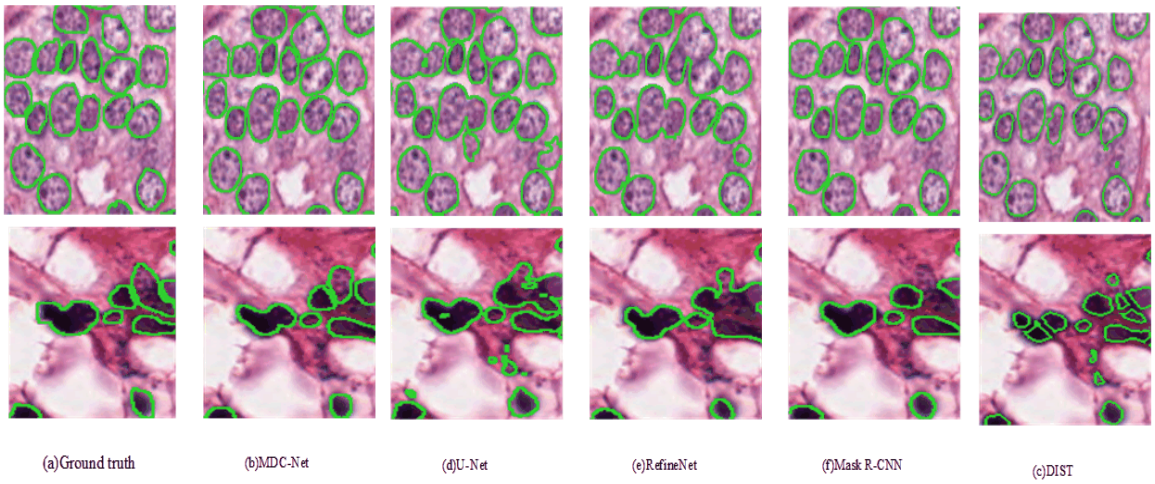

Figure 7: The results which obtain by using different method, and each column is the result which different segmentation method, and MDC-Net is shown in second column.

that MDC-Net using distance map and contour information can obtain better segmentation results. The reason is MDC-Net which can enhance morphology and boundary information of individual nuclei.

4.5.2. Evaluation influences for every part

We evaluate the segmentation influences from different parts in the network. The dataset used DATA ORGANS. Setting t_0 and t_1 are 0.1 and 0.8, p_1 and p_2 are 1 and 0.1, respectively. We only compare on F1 score and AJI. The result of F1 and AJI in MDC-Net are 0.7859 and 0.5551, respectively. When remove the post-processing the F1 and AJI are 0.7845 and 0.5387, the F1 and AJI are 0.7816 and 0.5495 when using max-pooling layer to replace dilated convolution. When remove residual operation the F1 and AJI are 0.7737 and 0.5346, The ablation experiment demonstrate the residual operation has most significant effect in MDC-Net in all metrics. This show that fully use context information can have the most beneficial impact in our method on dense target segmentation task.

5. Conclusion

In this paper, we present a new fully convolutional network MDC-Net, and this is a nuclei segmentation method. Our target is to get the accurately segmentation result in image with overlapping and touching nucleus. Distance map and contour information are included in MDC-Net, it is used to enhance the nucleus morphological information and to highlight the nucleus boundary information. Furthermore, we use MDC-Net to get the segmentation result. In MDC-Net we use dilated convolution and multiple residual operations to reduce detail loss in image. Using fusion operation to fuse the predicted distance map and contour. Finally, using post-processing operation to improve segmentation result. The experimental

results prove that our proposed MDC-Net is superior to other state-of-the-art segmentation methods.

Acknowledgments

This research is partially supported by the National Natural Science Foundation of China under Grants 61403287, 61472293, and 61572381, and in part by the Natural Science Foundation of Hubei Province under Grant 2014CFB288.

References

Martín Abadi, Paul Barham, Jianmin Chen, Zhifeng Chen, Andy Davis, Jeffrey Dean, Matthieu Devin, Sanjay Ghemawat, Geoffrey Irving, Michael Isard, et al. Tensorflow: A system for large-scale machine learning. In *12th {USENIX} Symposium on Operating Systems Design and Implementation ({OSDI} 16)*, pages 265–283, 2016.

Mahmoud Abdolhoseini, Murielle G Kluge, Frederick R Walker, and Sarah J Johnson. Segmentation of heavily clustered nuclei from histopathological images. *Scientific reports*, 9(1):4551, 2019.

Yousef Al-Kofahi, Alla Zaltsman, Robert Graves, Will Marshall, and Mirabela Rusu. A deep learning-based algorithm for 2-d cell segmentation in microscopy images. *BMC bioinformatics*, 19(1):365.

Hao Chen, Xiaojuan Qi, Lequan Yu, and Pheng-Ann Heng. Dcan: deep contour-aware networks for accurate gland segmentation. In *Proceedings of the IEEE conference on Computer Vision and Pattern Recognition*, pages 2487–2496, 2016.

Liang-Chieh Chen, George Papandreou, Florian Schroff, and Hartwig Adam. Rethinking atrous convolution for semantic image segmentation. *arXiv preprint arXiv:1706.05587*, 2017.

Jierong Cheng, Jagath C Rajapakse, et al. Segmentation of clustered nuclei with shape markers and marking function. *IEEE Transactions on Biomedical Engineering*, 56(3): 741–748, 2008.

Matthew C Clark, Lawrence O Hall, Dmitry B Goldgof, Laurence P Clarke, Robert P Velthuizen, and Martin S Silbiger. Mri segmentation using fuzzy clustering techniques. *IEEE Engineering in Medicine and Biology Magazine*, 13(5):730–742, 1994.

Larry S Davis. A survey of edge detection techniques. *Computer graphics and image processing*, 4(3):248–270, 1975.

Yuncong Feng, Haiying Zhao, Xiongfei Li, Xiaoli Zhang, and Hongpeng Li. A multi-scale 3d otsu thresholding algorithm for medical image segmentation. *Digital Signal Processing*, 60:186–199, 2017.

Paweł Filipczuk, Thomas Fevens, Adam Krzyżak, and Roman Monczak. Computer-aided breast cancer diagnosis based on the analysis of cytological images of fine needle biopsies. *IEEE Transactions on Medical Imaging*, 32(12):2169–2178, 2013.

Yi Gao, Vadim Ratner, Liangjia Zhu, Tammy Diprima, Tahsin Kurc, Allen Tannenbaum, and Joel Saltz. Hierarchical nucleus segmentation in digital pathology images. In *Medical Imaging 2016: Digital Pathology*, volume 9791, page 979117. International Society for Optics and Photonics, 2016.

Peifang Guo, Alan Evans, and Prabir Bhattacharya. Segmentation of nuclei in digital pathology images. In *2016 IEEE 15th International Conference on Cognitive Informatics & Cognitive Computing (ICCI* CC)*, pages 547–550. IEEE, 2016.

Daniel P Huttenlocher, William J Rucklidge, and Gregory A Klanderman. Comparing images using the hausdorff distance under translation. In *Proceedings 1992 IEEE Computer Society Conference on Computer Vision and Pattern Recognition*, pages 654–656. IEEE, 1992.

Andrew Janowczyk and Anant Madabhushi. Deep learning for digital pathology image analysis: A comprehensive tutorial with selected use cases. *Journal of pathology informatics*, 7, 2016.

Zhipeng Jia, Xingyi Huang, I Eric, Chao Chang, and Yan Xu. Constrained deep weak supervision for histopathology image segmentation. *IEEE transactions on medical imaging*, 36(11):2376–2388, 2017.

Neeraj Kumar, Ruchika Verma, Sanuj Sharma, Surabhi Bhargava, Abhishek Vahadane, and Amit Sethi. A dataset and a technique for generalized nuclear segmentation for computational pathology. *IEEE transactions on medical imaging*, 36(7):1550–1560, 2017.

Guosheng Lin, Anton Milan, Chunhua Shen, and Ian Reid. Refinenet: Multi-path refinement networks for high-resolution semantic segmentation. In *Proceedings of the IEEE conference on computer vision and pattern recognition*, pages 1925–1934, 2017.

X. Liu, T. Fu, Z. Pan, D. Liu, W. Hu, J. Liu, and K. Zhang. Automated layer segmentation of retinal optical coherence tomography images using a deep feature enhanced structured random forests classifier. *IEEE Journal of Biomedical and Health Informatics*, 23(4): 1404–1416, July 2019. ISSN 2168-2194. doi: 10.1109/JBHI.2018.2856276.

Xiaoming Liu, Jun Cao, Tianyu Fu, Zhifang Pan, Wei Hu, Kai Zhang, and Jun Liu. Semi-supervised automatic segmentation of layer and fluid region in retinal optical coherence tomography images using adversarial learning. *IEEE Access*, 7:3046–3061, 2018.

Shivang Naik, Scott Doyle, Shannon Agner, Anant Madabhushi, Michael Feldman, and John Tomaszewski. Automated gland and nuclei segmentation for grading of prostate and breast cancer histopathology. In *2008 5th IEEE International Symposium on Biomedical Imaging: From Nano to Macro*, pages 284–287. IEEE, 2008.

Peter Naylor, Marick Laé, Fabien Reyal, and Thomas Walter. Segmentation of nuclei in histopathology images by deep regression of the distance map. *IEEE transactions on medical imaging*, 38(2):448–459, 2018.

Shan E Ahmed Raza, Linda Cheung, Muhammad Shaban, Simon Graham, David Epstein, Stella Pelengaris, Michael Khan, and Nasir M Rajpoot. Micro-net: A unified model for segmentation of various objects in microscopy images. *Medical image analysis*, 52: 160–173, 2019.

Olaf Ronneberger, Philipp Fischer, and Thomas Brox. U-net: Convolutional networks for biomedical image segmentation. In *International Conference on Medical image computing and computer-assisted intervention*, pages 234–241. Springer, 2015.

Korsuk Sirinukunwattana, Shan e Ahmed Raza, Yee-Wah Tsang, David RJ Snead, Ian A Cree, and Nasir M Rajpoot. Locality sensitive deep learning for detection and classification of nuclei in routine colon cancer histology images. *IEEE Trans. Med. Imaging*, 35 (5):1196–1206, 2016.

Pierre Soille. *Morphological image analysis: principles and applications*. Springer Science & Business Media, 2013.

Fuyong Xing and Lin Yang. Robust nucleus/cell detection and segmentation in digital pathology and microscopy images: a comprehensive review. *IEEE reviews in biomedical engineering*, 9:234–263, 2016.

Jun Xu, Lei Xiang, Qingshan Liu, Hannah Gilmore, Jianzhong Wu, Jinghai Tang, and Anant Madabhushi. Stacked sparse autoencoder (ssae) for nuclei detection on breast cancer histopathology images. *IEEE transactions on medical imaging*, 35(1):119–130, 2015.

Xiaodong Yang, Houqiang Li, and Xiaobo Zhou. Nuclei segmentation using marker-controlled watershed, tracking using mean-shift, and kalman filter in time-lapse microscopy. *IEEE Transactions on Circuits and Systems I: Regular Papers*, 53(11):2405–2414, 2006.

Fisher Yu and Vladlen Koltun. Multi-scale context aggregation by dilated convolutions. *arXiv preprint arXiv:1511.07122*, 2015.